CO_2 Activation on Ni(111) and Ni(100) Surfaces in the Presence of H_2O: An Ambient-Pressure X-ray Photoelectron Spectroscopy Study

Jun Cai,[†,‡,∥,⊥] Yong Han,[‡,⊥] Shuyue Chen,[‡] Ethan J. Crumlin,[§] Bo Yang,[*,‡] Yimin Li,[*,†,‡] and Zhi Liu[*,†,‡]

[†]State Key Laboratory of Functional Materials for Informatics, Shanghai Institute of Microsystem and Information Technology, Chinese Academy of Sciences, Shanghai 200050, China

[‡]School of Physical Science and Technology, ShanghaiTech University, Shanghai 201210, China

[§]Advanced Light Source, Lawrence Berkeley National Laboratory, Berkeley, California 94720, United States

[∥]University of Chinese Academy of Sciences, Beijing 100049, China

ABSTRACT: Nickel-based catalysts play an important role in the chemical transformation of CO_2. A fundamental understanding of the interaction between CO_2 and Ni surfaces at atomic level is necessary. In this study, the interfacial reactions of CO_2 and CO_2 + H_2O mixture on Ni(111) as well Ni(100) surfaces were investigated using ambient pressure X-ray photoelectron spectroscopy as well as theoretical calculations. The results indicate that the distributions of dissociation products are very different on the Ni(111) and Ni(100) surfaces. Carbonate, CO, and graphitic carbon formed on both Ni(111) and Ni(100) surfaces in the presence of 0.2 Torr CO_2. However, more than 90% adsorption species on the Ni(111) surface is the carbonate, whereas the Ni(100) surface is mainly covered by adsorbed CO* and graphitic carbon. The co-adsorption of H_2O weakens the influence of structure effect on the interfacial interaction between CO_2 and Ni surfaces. Furthermore, the density functional theory calculations suggest that the activation of CO_2 on Ni(111) and Ni(100) tends to follow different reaction paths, which are consistent with the experimental results.

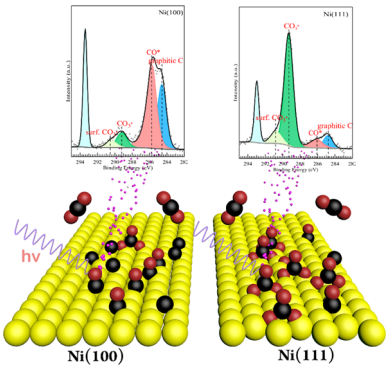

INTRODUCTION

The CO_2 emission from the excessive use of fossil fuels had led to serious environmental issues, such as global warming. Catalytic reduction of CO_2 to high-value-added chemicals and fuels is one of the promising approaches for CO_2 sequestration.[1−4] A major challenge in this field is developing low-cost transition metal catalysts, such as Ni, Co, and Cu,[5−9] for highly selective hydrogenation and photo/electrochemical reductions.[2,4,10,11]

Among earth-abundant catalytic materials, Ni is one of the top candidates for CO_2 reduction through methanation or methanol synthesis.[9,12−16] In these reactions, structure sensitivity is believed to play a key role in determining the reaction mechanism and product selectivity. For CO_2 hydrogenation process, Vogt recently demonstrated that the reaction activity and pathway change markedly with particle size.[13]

Theoretical studies suggest that surface orientation affects the activation of CO_2 on Ni by altering the energetics for subsequential C−O bond breakage.[17] Recently, the activation of CO_2 on the model Ni catalyst surfaces, Ni(111) and Ni(110), has been investigated separately by two research groups using ambient pressure X-ray photoelectron spectroscopy (APXPS) in situ technique.[18−20] On the compact surface, carbonate is identified as the dominating surface intermediate by Heine at room temperature.[18] On the open surface, graphitic carbon is the major surface species as shown by Roiaz and Monachino at elevated temperature at 425 K.[19,20] However, the excessive amount of graphitic carbon on Ni(110) is still under doubt, since they may be produced by the heating filament at high temperatures.[18]

In this work, the structure sensitivity of CO_2 activation is systematically investigated on the Ni(111) and Ni(100) model surfaces using APXPS and density functional theory (DFT) simulations. Our APXPS results show that, even at room temperature, the Ni(100) surface is capable of breaking C−O bonds to produce graphitic carbon with about 30% surface coverage. In stark contrast, the dominant surface species is carbonate on the compact (111) surface. These observations are further corroborated by DFT calculations of the energetics of competing elementary processes. Moreover, the subsequent addition of H_2O on the Ni surfaces induces marked changes in the distribution of surface species.

EXPERIMENTAL SECTION

The APXPS experiments were carried out at Beamline 9.3.2 of the Advanced Light Source at Lawrence Berkeley National

Laboratory.[21] Before the experiments, the APXPS chamber was baked at 120 °C for 48 h, achieving a base pressure of 8 × 10^{-10} Torr. The nickel single crystals were cleaned by several cycles of Ar^+ sputtering (2 keV, 15 mA) and annealing at 600 °C.[22,23] The clean Ni(111) and Ni(110) surfaces were produced, as verified by the XPS spectra and low-energy electron diffraction (LEED) (Figure S1). H_2O (research grade) was purified by repeated freeze−pump−thaw cycles.[24] To minimize contamination, the gas lines for CO_2 and H_2O were baked at 120 °C for 2 h and flushed several times using high-purity CO_2 (99.999%) or H_2O before introducing CO_2 or H_2O into the chamber.

Incident photon energy ($E_{h\nu}$) of 410 eV for C 1s and 650 eV for O 1s were used to produce ejected photoelectrons with kinetic energy (E_{kin}) ~120 eV, corresponding to electron inelastic mean free path of around 0.43 nm.[25] Unless otherwise stated, the spectra were fitted by Casa XPS software using a Shirly-type background. The symmetrical peaks were fitted using the GL(30) line shape (a mixing of 70% Gaussian and 30% Lorentzian), whereas the asymmetric Ni 3p peaks were fitted using the DS(0.02,100)GL(30) line shape, a hybrid Doniach Sunjic/Gaussian−Lorentzian (product).[26] The detailed fitting procedure is given in Section IV of the Supporting Information (SI).

All DFT calculations were performed with Vienna ab initio simulation package.[27−29] The revised Perdew−Burke−Ernzerhof (RPBE) functional was used to describe the electron−ion interaction in projector-augmented wave approach.[30−33] Spin polarization was taken into consideration due to the magnetism of nickel, and the electron occupancy was determined using Methfessel−Paxton scheme with a smearing width of 0.1 eV.[34] Adsorption geometries were optimized using a force-based conjugate gradient algorithm, whereas transition states (TSs) were located with a constrained minimization method.[35−37] The force convergence was set to 0.05 eV/Å with a total energy convergence of 10^{-4} eV and the energy cutoff for the plane-wave expansion was set to 500 eV. The Ni(111) and (100) surfaces were modeled as a periodic four-layer slab with half of the layers fixed at their bulk positions. The $p(3 \times 3)$ supercell was chosen with a $(4 \times 4 \times 1)$ Monkhorst−Pack k-point mesh for Ni(111) and $(3 \times 3 \times 1)$ for Ni(100).[38] A vacuum spacing of more than 15 Å was placed above the surface. The adsorption energy was calculated using the equation: $E_{ad} = E_{A/S} - E_S - E_A$. $E_{A/S}$ and E_S represent the energies of the slab with and without the adsorbate, respectively, and E_A represents the adsorbate energy in the gas phase. Previous research shows that the DFT calculation of the carbon−oxygen double bond has a systematic error, and the correction for RPBE is +0.41 eV for the gaseous CO_2.[39]

RESULTS AND DISCUSSION

CO_2 Adsorption on Different Ni Single-Crystal Surfaces.

To study the influence of surface orientation on the CO_2 activation, Ni(111) and Ni(100) surfaces were exposed to CO_2 in the main chamber at room temperature. Figure 1a,b show the C 1s spectra of the surfaces species on Ni(111) and Ni(100) in the presence of 0.2 Torr CO_2, respectively. The C 1s spectra exhibit three main spectral regions: (i) the peak with binding energy (BE) of 293.0 eV comes from the CO_2 gas phase; (ii) the peaks located at 288.8 and 290.0 eV are attributed to two kinds of carbonate species ("carbonate I" and "carbonate II");[18,40] (iii) the peaks with

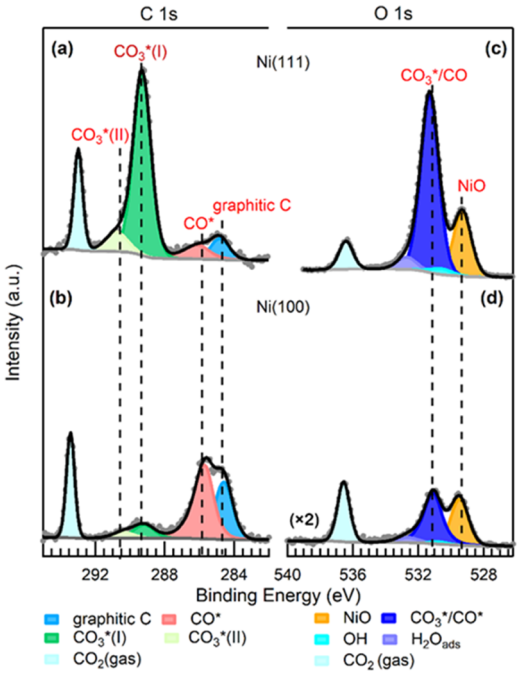

Figure 1. (a, b) C 1s spectra on Ni(111) and Ni(100), respectively, and (c) and (d) the corresponding O 1s spectra. The O 1s spectrum in (d) is scaled by a factor of 2 for clarity. CO_2 adsorption was performed in 0.2 Torr CO_2 at room temperature. All of the spectra were collected with a photoelectron kinetic energy of 120 eV.

BEs of 284.8 and 285.6 eV can be assigned to the graphitic carbon and adsorbed CO (CO*), respectively.[18,41−43]

Figure 1c,d show the O 1s spectra of the adsorption species on the Ni(111) and Ni(100) surfaces in the presence of 0.2 Torr CO_2, respectively. The peaks with BEs of 536.6 and 529.5 eV are assigned to the gas phase CO_2 and NiO, respectively.[44] The O 1s peak at 531.1 eV can be attributed to both CO* and carbonate species.[18,20] The peaks with BEs of 532.7 and 530.8 eV are attributed to the adsorbed H_2O and hydroxy (OH).[45,46] The presence of H_2O and OH on the Ni surfaces is due to the H_2O background pressure. The effect of H_2O on the adsorbed species will be discussed later.

Compared with that in the ultra-high vacuum (UHV) conditions, the adsorption and dissociation of CO_2 on Ni surfaces under ambient pressure conditions show a significant difference. The previous UHV studies indicate that the linear CO_2 is physisorbed on the Ni(110) and Ni(100) surfaces at 100 K, and it transforms into bent chemisorbed CO_2 (CO_2*) at 120−200 K.[23,47,48] The CO_2* further dissociates into CO* and atomic oxygen above 200 K. In addition, only physisorbed CO_2 is formed on the Ni(111) surface below 100 K. Neither chemisorbed CO_2 nor dissociated CO_2 is observed above 120 K on this surface.[47] From Figure 1, in addition to carbonate, CO* and graphitic carbon species are found on both Ni(111) and Ni(100) surfaces in the presence of 0.2 Torr CO_2. However, there is no peak related to CO_2* (with BE of 286−287 eV), which results from the unstable state of CO_2* above 220 K.[48]

Heine et al. previously reported that two carbonate species, corresponding to two C 1s peaks at 288.9 and 289.7 eV, formed on the Ni(111) surface under 0.2 Torr CO_2 at room temperature.[18] In our study, we started the scan of C 1s spectra immediately after the introduction of CO_2. A peak around 288.8 eV appeared on the Ni(111) surface at the beginning (as

shown in Figure S2). A small amount of CO* and graphitic carbon appeared when the pressure was stable at 0.2 Torr (~30 min after introducing CO_2). The minor difference between our work and previous study (CO* and graphitic carbon) could be a result of the defect sites and/or steps on the Ni(111) surface (shown in Figure S1). The possible beam-induced effect was evaluated by collecting the spectra at two spots with different irradiating time. The results (Figure S3) indicated that the beam-induced effect was negligible in our experiment.

On Ni(111), two C 1s peaks with BEs at 288.8 eV (carbonate I) and 290.0 eV (carbonate II) can be identified (Figure 1a). The depth-profile XPS experiments carried out using the photoelectron kinetic energies (E_{kin}) at 120 and 360 eV (Figure S4) indicate that carbonate II is slightly surface rich. This difference is not sufficient for a clear bulk and surface assignment.[18] Therefore, we assign them as two different carbonate species found on the surface. These results are consistent with previous studies.[18] Figure 1b shows that the peak intensities of the carbonate species on Ni(100) are substantially weaker than those on Ni(111). However, carbonate I and carbonate II species can still be resolved in our XPS analysis.

Even though the CO_2 adsorption on Ni(110) and Ni(100) surfaces is similar under UHV conditions, our results indicate that CO_2 adsorption on Ni(100) is different from that on Ni(110) under ambient pressure conditions.[49] We find that the Ni(100) surface is covered by adsorbed CO*, graphitic carbon, and a little carbonate. However, the carbonate, two CO species, and three graphitic carbon species are observed on the Ni(110) surface in 0.01 mbar CO_2 at 425 K.[19] The difference could be a result of difference in the reactivities between the Ni(110) and Ni(100) surfaces.

The significant difference in the distribution of adsorbed species on Ni(100) and Ni(111) surfaces is attributed to the fact that the dissociation of CO_2 on these two surfaces tends to follow different reaction routes. According to the peak intensities of each species from C 1s spectra (shown in Figure 1a,b), we can calculate the relative concentration of different surface carbon species. As shown in Figure S5, the major species on Ni(100) are adsorbed CO* (54%, relative content) and graphitic carbon (33%). However, the dominant species on Ni(111) is carbonate (73%), with a small amount of graphitic carbon (10%) and CO* (17%). The adsorbed CO* originates from the dissociation of CO_2 ($CO_2 \rightarrow CO^* + O^*$). Then, the reaction of O* with CO_2* leads to the formation of the carbonate ($O^* + CO_2^* \rightarrow CO_3^*$). The graphitic carbon comes from the further dissociation of CO* ($CO^* \rightarrow C^* + O^*$). On both Ni(111) and Ni(100) surfaces, the first reaction step is the cleavage of the C−O bond in CO_2 ($CO_2^* \rightarrow CO^* + O^*$). Then, on the Ni(111) surface, the reaction between atomic oxygen and adsorbed CO_2 leads to the formation of carbonate. However, on the Ni(100) surface, the next step is the decomposition of CO* rather than the formation of carbonate.

To understand these experimental findings, we performed DFT calculations to compare the activation barriers and reaction energies of elementary steps, namely, the dissociation of CO_2 to CO* and O*, the dissociation of CO* to graphitic carbon and oxygen, and the oxidation of CO_2 to produce CO_3*, on Ni(111) and Ni(100). To see more clearly how CO_2 dissociates on the surfaces, the transition state (TS) configurations are plotted in Figure 2 and the reaction barriers

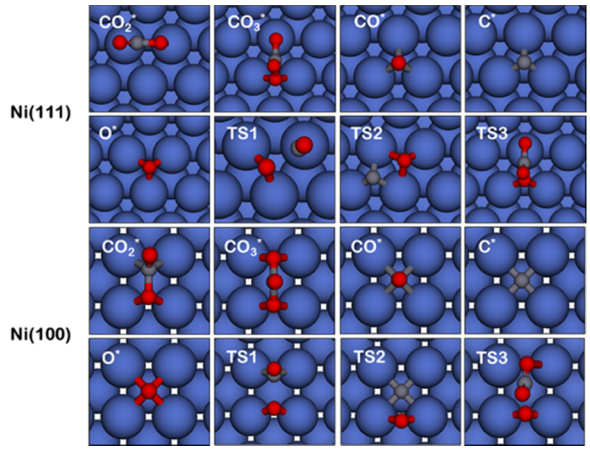

Figure 2. Structure of adsorbates and transition states on Ni(111) and Ni(100). CO_2*, CO_3*, CO*, C*, O*, and TS1 for CO_2* dissociation, TS2 for CO* dissociation, and TS3 for CO_3* formation.

are shown in Table 1. As one can see from Table 1, the adsorption of CO_2 on Ni(100) is much stronger than that on

Table 1. Reaction Barriers and Reaction Energies of Elementary Steps on Ni(111) and Ni(100) Surfaces

reactions	E_a(111)	ΔE(111)	E_a(100)	ΔE(100)
$CO_2 \rightarrow CO_2^*$		0.11		−0.27
$CO_2^* \rightarrow CO^* + O^*$	1.34	−1.08	0.33	−1.02
$CO^* \rightarrow C^* + O^*$	3.15	1.42	1.96	−0.18
$O^* + CO_2^* \rightarrow CO_3^*$	0.65	0.40	1.05	0.29

Ni(111), and the subsequent dissociation of CO_2 is much easier on Ni(100). The difference between the activation energies of CO_2 dissociation to CO* and O* on these two surfaces is as high as 1.01 eV. Further dissociation of CO gives rise to high barriers of 3.15 and 1.96 eV on Ni(111) and Ni(100), respectively, indicating that this step is relatively slow but the barrier is also much lower on Ni(100). It is interesting to see that there is competition between the dissociation and oxidation of CO_2 on the two surfaces, and the preferred reaction pathways are different on these two surfaces studied. On Ni(111), the barrier for CO_2 dissociation is much higher than the barrier for CO_2 oxidation, whereas the dissociation of CO_2 gives rise to a much lower barrier on Ni(100), this is consistent with the results observed experimentally that the formation of carbonate is ready to take place on Ni(111), whereas the dissociation of CO_2 and CO is preferred on Ni(100).

Figure 1a shows that the total amount of carbonates is much higher than that of CO*. The formation of carbonate follows these two elemental steps: (1) $CO_2^* \rightarrow CO^* + O^*$ and (2) $O^* + CO_2^* \rightarrow CO_3^*$. If all of the dissociation products stay on the Ni surface, the content of carbonate should not be higher than that of CO*. Hence, a substantial amount of CO* must be desorbed from the carbonate- and O-covered Ni(111) surface. The desorption of certain carbon-rich species with O/C < 2 is also confirmed by the calculation of the atomic ratio of O/C of the adsorption species.

The semiquantitative analysis of the species on Ni(111) and Ni(100) (as shown in Section VII of the SI) indicates that the O/C ratio of adsorption species on Ni(111) (~4.5) is higher than that of CO_2 stoichiometric ratio (2.0), which means that

O accumulation occurred on the Ni(111) surface during the reaction. CO* is the most likely desorption species, since the desorption of graphitic carbon is impossible at room temperature.

The large amount of CO desorbed at room temperature during the CO_2 activation on Ni(111) seems to contradict to the strong adsorption of CO on Ni(111). However, under 0.2 Torr, the other co-adsorbed species, oxygen and carbonate, are energetically more stable than CO*. For example, the adsorption energy of oxygen on clean Ni(111) is about 2 times higher than that of CO*.[50,51] Therefore, the co-adsorption of these species at high pressures can significantly weaken CO adsorption.

On Ni(100), the O/C ratio of 1.9 is close to that of CO_2 molecule, indicating that the desorption of CO* is negligible on this surface. According to our DFT calculations (Table 1), surface oxygen on Ni(100) has very low reactivity with chemisorbed CO_2 to form carbonate, and the strongly adsorbed CO* can easily dissociate into stable carbon and oxygen on the surface. The lack of carbonate formation makes more surface sites available for CO* adsorption and its further dissociation.

H_2O and CO_2 Co-adsorption on Ni(111) and Ni(100) Surface. Water always plays an important role in the real catalytic reactions. Humidity change induces significant differences in both the surface species and surface chemical state of Ni. To study the effect of H_2O on CO_2-predosed Ni surfaces, 0.2 Torr H_2O was introduced into the chamber after the pressure of CO_2 was stabilized at 0.2 Torr. The C 1s and O 1s spectra of Ni(111) as well as Ni(100) under 0.2 Torr CO_2 + 0.2 Torr H_2O are shown in Figure 3.

In the O 1s spectra (Figure 3c,d), the new peak at 535.3 eV originates from the gas-phase H_2O. The intensities of peaks at 530.9 eV (hydroxyl) and 532.6 eV (adsorbed water) increase obviously, indicating that the adsorption and dissociation of

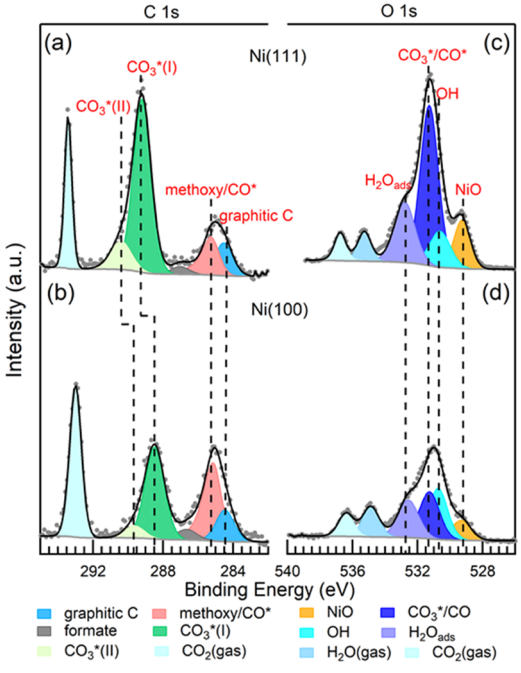

Figure 3. (a) C 1s and (c) O 1s spectra of Ni(111) and (b) C 1s and (d) O 1s spectra of Ni(100) in 0.2 Torr CO_2 + 0.2 Torr H_2O at room temperature.

H_2O occur on the Ni surfaces. The dissociation products, hydrogen and hydroxyl, further react with CO_2 and other surface species to produce formate, methoxy, and carbonate species.[52]

In the C 1s spectra (Figure 3a,b), the new peak at 287.0 eV can be assigned to formate,[52] one of the CO_2 hydrogenation products. The formation of methoxy species cannot be clearly resolved because its C 1s peak position (285.6 eV) is same as that of CO*. If we assume that the introduction of H_2O on the Ni surface predosed with CO_2 has a small effect on the surface concentration of graphitic carbon, the surface concentration changes of the other carbon-containing species can be estimated by using the peak intensity of graphitic carbon as a normalization constant (Figure 4). An increase of this peak

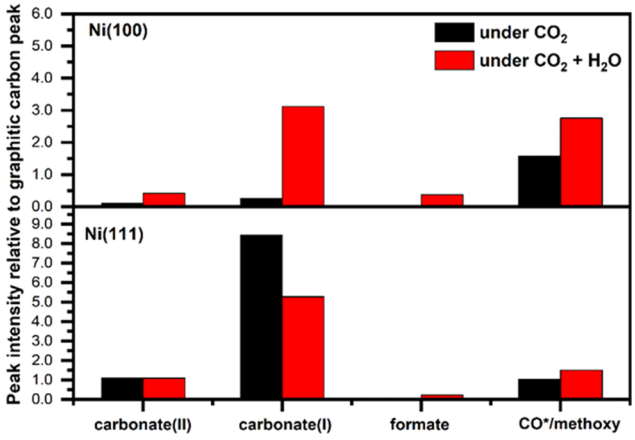

Figure 4. H_2O-induced effects on carbon-containing species on Ni(111) and Ni(100). The C 1s peak intensity of each species is normalized by the intensity of graphitic carbon on the same crystal surface under the same reaction condition.

intensity at 285.6 eV is found on both Ni(111) and Ni(100) surfaces. Since the Ni surfaces become more oxidized after dosing with water (shown in Figure S7), and CO does not adsorb on the NiO or $NiCO_3$ surfaces at room temperature,[18] we attribute this increase of peak intensities to methoxy formation.[24,53]

H_2O co-adsorption on the Ni surfaces has a prominent effect on carbonate species (Figure 4). On Ni(100), the surface concentration of carbonate increases dramatically. In contrast, the surface concentration of carbonate on Ni(111) decreases upon introducing H_2O. There is a shift of the carbonate peaks about 0.5 eV toward the higher binding energy on Ni(111) (Figure 3).

The reaction of metal-bound hydroxide with CO_2 to produce carbonate has been widely studied as an approach for CO_2 fixation. The study of hydroxo complexes of metal ion shows an order in the reactivity of various metals as Zn > Co ≫ Ni ≈ Mn > Cu ≈ 0.[54] A recent study further demonstrates that Ni−OH rapidly reacts with CO_2 to produce a carbonate species in the form of $Ni-OCO_2H$.[55] Therefore, this reaction should be responsible for the H_2O-induced increase of carbonate on Ni(100).

On Ni(111), there is an initial high surface concentration of carbonate before the addition of H_2O. Upon H_2O dissociation into hydrogen and OH, carbonate hydrogenation and formation are expected to compete with each other. The steady-state surface concentration of carbonate should be

determined by the initial surface concentration and the rates of carbonate hydrogenation and formation. Similar to Ni(111), a H_2O-induced decrease of carbonate concentration has been observed previously on a carbonate-covered Co surface.

After H_2O addition, formate appears in a small amount on both Ni(111) and Ni(100) (Figure 3a,b), which suggests that, unlike Cu, hydrogenation of chemisorbed $CO_2^{\delta-}$ to formate is not a favorable reaction path on the Ni surfaces.[56,57] Methoxy can be formed by hydrogenation of formate and carbonate.[58] The amount of methoxy formed cannot be determined in this XPS study due to the peak overlap of methoxy and CO*.

Finally, our analysis of H_2O-induced effect is based on the assumption that the change in surface concentration of graphitic carbon is small enough to be neglected. We believe that this is reasonable assumption on the CO_2-predosed surfaces at room temperature.

CONCLUSIONS

In this work, CO_2 activation and subsequent H_2O-induced effects on Ni(111) and Ni(100) are studied by APXPS and DFT calculation. Our results show that the surface orientation of Ni has a profound influence on the reaction pathway for CO_2 activation. Under 0.2 Torr of CO_2 and room temperature, carbonate species are the dominant surface intermediates on Ni(111). However, on Ni(100), adsorbed CO* and graphitic carbon are the major surface species. DFT calculations unveil that CO_2* chemisorbed on Ni(111) has a low activation energy to react with surface oxygen to form carbonate, and that, on Ni(100), the sequential C−O bond cleavage of CO_2* dissociation is energetically favorable.

Formate and methoxy are resolved by APXPS after introducing 0.2 Torr of H_2O to the CO_2-dosed Ni surfaces. Prominent changes in the surface concentration of carbonate are observed on both Ni(111) and Ni(100). On Ni(100), the concentration increases significantly. However, on Ni(111), the concentration decreases. We attribute these observations to the competition between carbonate hydrogenation by hydrogen and formation through the reaction of Ni−OH and CO_2.

AUTHOR INFORMATION

Corresponding Authors

*E-mail: yangbo1@shanghaitech.edu.cn (B.Y.).
*E-mail: liym1@shanghaitech.edu.cn (Y.L.).
*E-mail: zliu2@mail.sim.ac.cn (Z.L.).

ORCID

Ethan J. Crumlin: 0000-0003-3132-190X
Bo Yang: 0000-0001-6904-6646
Zhi Liu: 0000-0002-8973-6561

Author Contributions

⊥J.C. and Y.H. contributed equally.

Notes

The authors declare no competing financial interest.

ACKNOWLEDGMENTS

The part of this work performed in China was supported by the National Natural Science Foundation of China (11227902, 21802096, and 21832004) and the Science and Technology Commission of Shanghai Municipality (14520722100). Y.L. would like to acknowledge the support of the "Hundred Talents Program" of the Chinese Academy of Sciences. B.Y. would like to thank the HPC Platform of ShanghaiTech University for computing time. The work performed at the Advanced Light Source is supported by the Director, Office of Science, Office of Basic Energy Sciences of the U.S. Department of Energy under Contract No. DE-AC02-05CH11231.

REFERENCES

(1) Aresta, M.; Dibenedetto, A.; Angelini, A. Catalysis for the valorization of exhaust carbon: from CO_2 to chemicals, materials, and fuels. Technological use of CO_2. *Chem. Rev.* **2014**, *114*, 1709−1742.

(2) Álvarez, A.; Bansode, A.; Urakawa, A.; Bavykina, A. V.; Wezendonk, T. A.; Makkee, M.; Gascon, J.; Kapteijn, F. Challenges in the greener production of formates/formic acid, methanol, and DME by heterogeneously catalyzed CO_2 hydrogenation processes. *Chem. Rev.* **2017**, *117*, 9804−9838.

(3) Li, W.; Wang, H.; Jiang, X.; Zhu, J.; Liu, Z.; Guo, X.; Song, C. A short review of recent advances in CO_2 hydrogenation to hydrocarbons over heterogeneous catalysts. *RSC Adv.* **2018**, *8*, 7651−7669.

(4) Porosoff, M. D.; Yan, B.; Chen, J. G. Catalytic reduction of CO_2 by H_2 for synthesis of CO, methanol and hydrocarbons: challenges and opportunities. *Energy Environ. Sci.* **2016**, *9*, 62−73.

(5) Kattel, S.; Liu, P.; Chen, J. G. Tuning selectivity of CO_2 hydrogenation reactions at the metal/oxide interface. *J. Am. Chem. Soc.* **2017**, *139*, 9739−9754.

(6) Dinh, C.-T.; Burdyny, T.; Kibria, M. G.; Seifitokaldani, A.; Gabardo, C. M.; de Arquer, F. P. G.; Kiani, A.; Edwards, J. P.; De Luna, P.; Bushuyev, O. S.; et al. CO_2 electroreduction to ethylene via hydroxide-mediated copper catalysis at an abrupt interface. *Science* **2018**, *360*, 783−787.

(7) Graciani, J.; Mudiyanselage, K.; Xu, F.; Baber, A. E.; Evans, J.; Senanayake, S. D.; Stacchiola, D. J.; Liu, P.; Hrbek, J.; Sanz, J. F.; Rodriguez, J. A. Highly active copper-ceria and copper-ceria-titania catalysts for methanol synthesis from CO_2. *Science* **2014**, *345*, 546−550.

(8) Gao, S.; Lin, Y.; Jiao, X.; Sun, Y.; Luo, Q.; Zhang, W.; Li, D.; Yang, J.; Xie, Y. Partially oxidized atomic cobalt layers for carbon dioxide electroreduction to liquid fuel. *Nature* **2016**, *529*, 68−71.

(9) Studt, F.; Sharafutdinov, I.; Abild-Pedersen, F.; Elkjær, C. F.; Hummelshøj, J. S.; Dahl, S.; Chorkendorff, I.; Nørskov, J. K. Discovery of a Ni-Ga catalyst for carbon dioxide reduction to methanol. *Nat. Chem.* **2014**, *6*, 320−324.

(10) Wang, W.; Wang, S.; Ma, X.; Gong, J. Recent advances in catalytic hydrogenation of carbon dioxide. *Chem. Soc. Rev.* **2011**, *40*, 3703−3727.

(11) Kondratenko, E. V.; Mul, G.; Baltrusaitis, J.; Larrazábal, G. O.; Pérez-Ramírez, J. Status and perspectives of CO_2 conversion into fuels and chemicals by catalytic, photocatalytic and electrocatalytic processes. *Energy Environ. Sci.* **2013**, *6*, 3112−3135.

(12) Keim, W. Nickel: an element with wide application in industrial homogeneous catalysis. *Angew. Chem., Int. Ed.* **1990**, *29*, 235−244.

(13) Vogt, C.; Groeneveld, E.; Kamsma, G.; Nachtegaal, M.; Lu, L.; Kiely, C. J.; Berben, P. H.; Meirer, F.; Weckhuysen, B. M. Unravelling structure sensitivity in CO_2 hydrogenation over nickel. *Nat. Catal.* **2018**, *1*, 127−134.

(14) Vesselli, E.; Schweicher, J.; Bundhoo, A.; Frennet, A.; Kruse, N. Catalytic CO_2 Hydrogenation on Nickel: Novel Insight by Chemical Transient Kinetics. *J. Phys. Chem. C* **2011**, *115*, 1255−1260.
(15) Du, G.; Lim, S.; Yang, Y.; Wang, C.; Pfefferle, L.; Haller, G. L. Methanation of carbon dioxide on Ni-incorporated MCM-41 catalysts: The influence of catalyst pretreatment and study of steady-state reaction. *J. Catal.* **2007**, *249*, 370−379.
(16) Weatherbee, G. D.; Bartholomew, C. H. Hydrogenation of CO_2 on group VIII metals: I. Specific activity of $NiSiO_2$. *J. Catal.* **1981**, *68*, 67−76.
(17) Wang, S.-G.; Cao, D.-B.; Li, Y.-W.; Wang, J.; Jiao, H. Chemisorption of CO_2 on nickel surfaces. *J. Phys. Chem. B* **2005**, *109*, 18956−18963.
(18) Heine, C.; Lechner, B. A.; Bluhm, H.; Salmeron, M. Recycling of CO_2: Probing the chemical state of the Ni(111) surface during the methanation reaction with ambient pressure x-ray photoelectron spectroscopy. *J. Am. Chem. Soc.* **2016**, *138*, 13246−13252.
(19) Roiaz, M.; Monachino, E.; Dri, C.; Greiner, M.; Knop-Gericke, A.; Schlögl, R.; Comelli, G.; Vesselli, E. Reverse Water−Gas Shift or Sabatier Methanation on Ni(110)? Stable Surface Species at Near-Ambient Pressure. *J. Am. Chem. Soc.* **2016**, *138*, 4146−4154.
(20) Monachino, E.; Greiner, M.; Knop-Gericke, A.; Schlögl, R.; Dri, C.; Vesselli, E.; Comelli, G. Reactivity of Carbon Dioxide on Nickel: Role of CO in the Competing Interplay between Oxygen and Graphene. *J. Phys. Chem. Lett.* **2014**, *5*, 1929−1934.
(21) Starr, D.; Liu, Z.; Hävecker, M.; Knop-Gericke, A.; Bluhm, H. Investigation of solid/vapor interfaces using ambient pressure X-ray photoelectron spectroscopy. *Chem. Soc. Rev.* **2013**, *42*, 5833−5857.
(22) Grosvenor, A. P.; Biesinger, M. C.; Smart, R. S. C.; McIntyre, N. S. New interpretations of XPS spectra of nickel metal and oxides. *Surf. Sci.* **2006**, *600*, 1771−1779.
(23) D'evelyn, M.; Hamza, A.; Gdowski, G.; Madix, R. Dynamics of the dissociative adsorption of CO_2 on Ni(100). *Surf. Sci.* **1986**, *167*, 451−473.
(24) Liu, Q.; Han, Y.; Cai, J.; Crumlin, E. J.; Li, Y.; Liu, Z. CO_2 Activation on Cobalt Surface in the Presence of H_2O: An Ambient-Pressure X-ray Photoelectron Spectroscopy Study. *Catal. Lett.* **2018**, *148*, 1686−1691.
(25) Shinotsuka, H.; Tanuma, S.; Powell, C.; Penn, D. Calculations of electron inelastic mean free paths. X. Data for 41 elemental solids over the 50 eV to 200 keV range with the relativistic full Penn algorithm. *Surf. Interface Anal.* **2015**, *47*, 871−888.
(26) Yuan, K.; Zhong, J.-Q.; Sun, S.; Ren, Y.; Zhang, J. L.; Chen, W. Reactive Intermediates or Inert Graphene? Temperature- and Pressure-Determined Evolution of Carbon in the CH_4−Ni(111) System. *ACS Catal.* **2017**, *7*, 6028−6037.
(27) Kresse, G.; Hafner, J. Abinitio Molecular-Dynamics for Liquid-Metals. *Phys. Rev. B* **1993**, *47*, 558−561.
(28) Kresse, G.; Hafner, J. Ab initio molecular-dynamics simulation of the liquid-metal−amorphous-semiconductor transition in germanium. *Phys. Rev. B* **1994**, *49*, 14251−14269.
(29) Kresse, G.; Furthmuller, J. Efficient iterative schemes for ab initio total-energy calculations using a plane-wave basis set. *Phys. Rev. B* **1996**, *54*, 11169−11186.
(30) Hammer, B.; Hansen, L. B.; Norskov, J. K. Improved adsorption energetics within density-functional theory using revised Perdew-Burke-Ernzerhof functionals. *Phys. Rev. B* **1999**, *59*, 7413−7421.
(31) Hammer, B.; Norskov, J. K. Theoretical Surface Science and Catalysis—Calculations and Concepts. In *Advances in Catalysis, Vol 45: Impact of Surface Science on Catalysis*; Gates, B. C.; Knozinger, H., Eds.; Elsevier Academic Press Inc: San Diego, 2000; Vol. *45*, pp 71−129.
(32) Blöchl, P. E. PROJECTOR AUGMENTED-WAVE METHOD. *Phys. Rev. B* **1994**, *50*, 17953−17979.
(33) Kresse, G.; Joubert, D. From ultrasoft pseudopotentials to the projector augmented-wave method. *Phys. Rev. B* **1999**, *59*, 1758−1775.
(34) Methfessel, M.; Paxton, A. T. High-precision sampling for Brillouin-zone integration in metals. *Phys. Rev. B* **1989**, *40*, 3616−3621.
(35) Alavi, A.; Hu, P.; Deutsch, T.; Silvestrelli, P. L.; Hutter, J. CO Oxidation on Pt(111): An Ab Initio Density Functional Theory Study. *Phys. Rev. Lett.* **1998**, *80*, 3650−3653.
(36) Liu, Z.-P.; Hu, P. General Rules for Predicting Where a Catalytic Reaction Should Occur on Metal Surfaces: A Density Functional Theory Study of C−H and C−O Bond Breaking/Making on Flat, Stepped, and Kinked Metal Surfaces. *J. Am. Chem. Soc.* **2003**, *125*, 1958−1967.
(37) Michaelides, A.; Liu, Z. P.; Zhang, C. J.; Alavi, A.; King, D. A.; Hu, P. Identification of General Linear Relationships between Activation Energies and Enthalpy Changes for Dissociation Reactions at Surfaces. *J. Am. Chem. Soc.* **2003**, *125*, 3704−3705.
(38) Chadi, D. J. Special points for Brillouin-zone integrations. *Phys. Rev. B* **1977**, *16*, 1746−1747.
(39) Peterson, A. A.; Abild-Pedersen, F.; Studt, F.; Rossmeisl, J.; Norskov, J. K. How copper catalyzes the electroreduction of carbon dioxide into hydrocarbon fuels. *Energy Environ. Sci.* **2010**, *3*, 1311−1315.
(40) Burghaus, U. Surface chemistry of CO_2 - Adsorption of carbon dioxide on clean surfaces at ultrahigh vacuum. *Prog. Surf. Sci.* **2014**, *89*, 161−217.
(41) Knudsen, J.; Merte, L. R.; Peng, G.; Vang, R. T.; Resta, A.; Lægsgaard, E.; Andersen, J. N.; Mavrikakis, M.; Besenbacher, F. Low-temperature CO oxidation on Ni(111) and on a Au/Ni(111) surface alloy. *ACS Nano* **2010**, *4*, 4380−4387.
(42) Peng, G.; Sibener, S.; Schatz, G. C.; Ceyer, S. T.; Mavrikakis, M. CO_2 hydrogenation to formic acid on Ni(111). *J. Phys. Chem. C* **2012**, *116*, 3001−3006.
(43) Held, G.; Schuler, J.; Sklarek, W.; Steinrück, H.-P. Determination of adsorption sites of pure and coadsorbed CO on Ni(111) by high resolution X-ray photoelectron spectroscopy. *Surf. Sci.* **1998**, *398*, 154−171.
(44) Payne, B.; Biesinger, M.; McIntyre, N. Use of oxygen/nickel ratios in the XPS characterisation of oxide phases on nickel metal and nickel alloy surfaces. *J. Electron Spectrosc. Relat. Phenom.* **2012**, *185*, 159−166.
(45) Mansour, A.; Melendres, C. Characterization of α-$Ni(OH)_2$ by XPS. *Surf. Sci. Spectra* **1994**, *3*, 255−262.
(46) Biesinger, M. C.; Payne, B. P.; Lau, L. W.; Gerson, A.; Smart, R. S. C. X-ray photoelectron spectroscopic chemical state quantification of mixed nickel metal, oxide and hydroxide systems. *Surf. Interface Anal.* **2009**, *41*, 324−332.
(47) Freund, H.-J.; Roberts, M. W. Surface chemistry of carbon dioxide. *Surf. Sci. Rep.* **1996**, *25*, 225−273.
(48) Wambach, J.; Illing, G.; Freund, H.-J. CO_2 activation and reaction with hydrogen on Ni(110): formate formation. *Chem. Phys. Lett.* **1991**, *184*, 239−244.
(49) Vesselli, E.; Rogatis, L. D.; Ding, X.; Baraldi, A.; Savio, L.; Vattuone, L.; Rocca, M.; Fornasiero, P.; Peressi, M.; Baldereschi, A.; et al. Carbon dioxide hydrogenation on Ni(110). *J. Am. Chem. Soc.* **2008**, *130*, 11417−11422.
(50) Stuckless, J.; Wartnaby, C.; Al-Sarraf, N.; Dixon-Warren, S. J.; Kovar, M.; King, D. A. Oxygen chemisorption and oxide film growth on Ni{100},{110}, and {111}: Sticking probabilities and microcalorimetric adsorption heats. *J. Chem. Phys.* **1997**, *106*, 2012−2030.
(51) Christmann, K.; Schober, O.; Ertl, G. Adsorption of CO on a Ni(111) surface. *J. Chem. Phys.* **1974**, *60*, 4719−4724.
(52) Vesselli, E.; Rizzi, M.; De Rogatis, L.; Ding, X.; Baraldi, A.; Comelli, G.; Savio, L.; Vattuone, L.; Rocca, M.; Fornasiero, P.; et al. Hydrogen-assisted transformation of CO_2 on nickel: the role of formate and carbon monoxide. *J. Phys. Chem. Lett.* **2010**, *1*, 402−406.
(53) Deng, X.; Verdaguer, A.; Herranz, T.; Weis, C.; Bluhm, H.; Salmeron, M. Surface chemistry of Cu in the presence of CO_2 and H_2O. *Langmuir* **2008**, *24*, 9474−9478.
(54) Kitajima, N.; Hikichi, S.; Tanaka, M.; Morooka, Y. Fixation of atmospheric carbon dioxide by a series of hydroxo complexes of

divalent metal ions and the implication for the catalytic role of metal ion in carbonic anhydrase. Synthesis, characterization, and molecular structure of [LM(OH)]n (n = 1 or 2) and LM(.mu.-CO3)ML (M(II) = Mn, Fe, Co, Ni, Cu, Zn; L = HB(3,5-iso-Pr2pz)3). *J. Am. Chem. Soc.* **1993**, *115*, 5496−5508.

(55) Huang, D.; Makhlynets, O. V.; Tan, L. L.; Lee, S. C.; Rybak-Akimova, E. V.; Holm, R. H. Kinetics and mechanistic analysis of an extremely rapid carbon dioxide fixation reaction. *Proc. Natl. Acad. Sci. U.S.A.* **2011**, *108*, 1222−1227.

(56) Bartholomew, C. H.; Farrauto, R. J. *Fundamentals of Industrial Catalytic Processes*; John Wiley & Sons, 2011.

(57) Yang, Y.; Mims, C. A.; Mei, D. H.; Peden, C. H. F.; Campbell, C. T. Mechanistic studies of methanol synthesis over Cu from CO/CO_2/H_2/H_2O mixtures: The source of C in methanol and the role of water. *J. Catal.* **2013**, *298*, 10−17.

(58) Grabow, L.; Mavrikakis, M. Mechanism of methanol synthesis on Cu through CO_2 and CO hydrogenation. *ACS Catal.* **2011**, *1*, 365−384.